Semiconductor Conduction Losses Prediction Considering the Current Ripple in a Three-Phase Two-Level Voltage Source Converter Driven by Different PWM Strategies

Daniel A. F. Collier and Marcelo L. Heldwein
Federal University of Santa Catarina (UFSC) — Electrical Engineering Department
Power Electronics Institute (INEP), P.O. box: 5119 — 88040-970 — Florianópolis/SC, BRAZIL
e-mail: collier@inep.ufsc.br; heldwein@inep.ufsc.br

***Abstract*—The choice of topologies, modulation strategies and semiconductors is a process that requires appropriatte tools to design a converter and to evaluate the technology to be employed. Typically, simulations are used to increase the precision during the analysis process of power converters. Theoretical tools to analyze three-phase voltage source converters (VSC) are given in depth in the bibliography, but some analyzes are based on simplifications and better results can still be determined. Applications of the VSC other than for power factor correction (PFC), such as drives applications, active filters, wind energy conversion, among others, require better theoretical results since most of the simplications are considered for PFC operation. Thus, a detailed analysis of the operation conditions has to be considered, which includes displacement angles, resistive voltage drops in wires and current ripples. In this work a detailed analysis of the current ripples in the phase current and in the semiconductor is presented for different PWM strategies. The switch models are considered for the most typical modern implementations, i.e., IGBT/diode and SiC MOSFET. A detailed comparison of the results for different PWM strategies and operation conditions is presented in order to highlight the improved accuracy of the proposed analysis.**

***Index Terms*—Power Factor Correction, PWM rectifiers, multi-state switching cells, high efficiency.**

I. Introduction

The choice of topologies, modulation strategies and semiconductors is a process that requires appropriatte tools to design a converter and to evaluate the technology to be employed. Typically, simulations are used to increase the precision during the analysis process of power converters [1]–[3]. Theoretical tools to analyze three-phase voltage source converters (VSC) (cf. Fig. 1(a)) are given in depth in [4], [5], but some analyzes are based on simplifications and better results can still be determined. Recent research in this subject [6] has presented a prediction of the current ripple in the phase current of a VSC, which has been employed to operate the VSC with variable frequency [7].

Applications of the VSC other than for power factor correction (PFC), such as drives applications, active filters, wind energy conversion, among others, require better theoretical results since most of the simplications are considered for PFC operation. Thus, a detailed analysis of the operation conditions has to be considered, which includes displacement angles, resistive voltage drops in wires and current ripples. In this work a detailed analysis of the current ripples in the phase current and in the semiconductor is presented for different PWM strategies. This is done considering the equivalent circuit of the VSC presented in Fig. 1(b), which takes into account the displacement angles and resistive voltage drops. The switch models are considered for the most typical modern implementations, i.e., IGBT/diode and SiC MOSFET. A detailed comparison of the results for different PWM strategies and operation conditions is presented in order to highlight the improved accuracy of the proposed analysis.

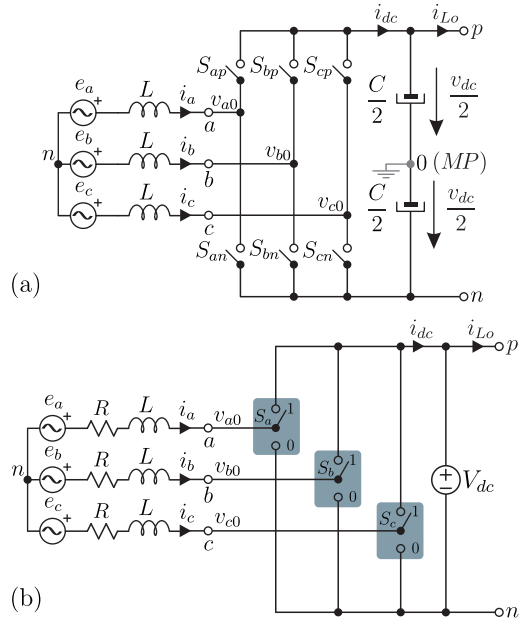

Fig. 1. (a) Three-phase two-level voltage source converter (VSC) topology; and, (b) Equivalent circuit diagram of the VSC including the ac-port resistive losses.

The choice of topologies, modulation strategies and semiconductors is a process that requires appropriatte tools to design a converter and to evaluate the technology to be employed. Typically, simulations are used to increase the precision during the analysis process of power converters [1]–[3]. Theoretical tools to analyze three-phase voltage source converters (VSC) (cf. Fig. 1(a)) are given in depth in [4], [5], but some analyzes are based on simplifications and better results can still be determined. Recent research in this subject [6] has presented a prediction of the current ripple in the phase current of a VSC, which has been employed to operate the VSC with variable frequency [7].

II. Analysis of the Conduction Losses Considering the Current Ripple

The instantaneous conduction losses p_X over a two-terminals circuit element X represented by a resistance r_X and a voltage drop v_X in this work is defined as

$$p_X = r_X i_X^2 + v_X i_X, \tag{1}$$

where i_X is the current across the element. An useful information regarding the conduction losses is its local average value [8], which for a signal y over a period T is defined by

$$\langle y \rangle_T = \frac{1}{T}\int_{t-T}^{t} y d\tau. \tag{2}$$

Thus, the local average value of the conduction losses over a switching period T_s if r_X and v_X are constant over a switching period is

$$\langle p_X \rangle_{T_s} = r_X \langle i_X \rangle_{T_s,rms}^2 + \langle v_X \rangle_{T_s} \langle i_X \rangle_{T_s}, \tag{3}$$

where $\langle i_X \rangle_{T_s,rms}$ is defined as the element current local rms value over a switching period [8].

An important aspect to employ (3) is the shape of the switched current i_X. Fig. 2 shows an hypothetical switched current over a switching period. This current is defined as

$$i_X = \langle i_X \rangle_{T_s} + \Delta i_X, \tag{4}$$

where Δi_X is the element current ripple peak-to-peak value. In this case, the current local average value does not change over a switching period and the average ripple is null.

In order to highlight the differences between the computed power losses taking into account the current ripple, the terms in (3) are expanded as $\langle p_X \rangle_{T_s} = p_X^{(r)} + p_X^{(v)}$, where the first term in the right hand side is the resistive losses (superscript (r))

$$p_X^{(r)} = r_X \langle i_X \rangle_{T_s,rms}^2 = p_{X,sim}^{(r)} + p_{X,rip}^{(r)} \tag{5}$$

and the second is the losses due the voltage drop (superscript (v))

$$p_X^{(v)} = \langle v_X \rangle_{T_s} \langle i_X \rangle_{T_s} = p_{X,sim}^{(v)} + p_{X,rip}^{(v)}. \tag{6}$$

They are also divided into the simplified current shape (subscript sim) losses, which is defined as the losses that are expected not taking in account the current ripple, and the ripple losses (subscript rip), which is due to the current ripple. Note that ripple induced losses in the voltage drop is always null since $\langle \Delta i_X \rangle_{T_s} = 0$. And, if half switching period was considered in the averages, the net expected result would be the same in a switching period.

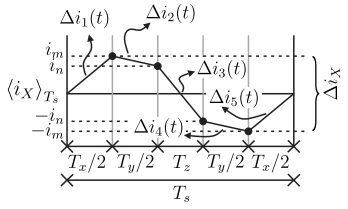

Fig. 2. Switched current i_X waveform in a switching period and its definitions.

The resistive simplified losses are computed with

$$p_{X,sim}^{(r)} = r_X \left(\frac{1}{T_s}\int_{t-T_s}^{t} (\langle i_X \rangle_{T_s})^2 d\tau \right) = r_X \langle i_{X,sim} \rangle_{T_s,rms}^2, \tag{7}$$

where $\langle i_{X,sim} \rangle_{T_s,rms}$ is the rms current value if no current ripple was considered. And, the resistive ripple induced losses with

$$p_{X,rip}^{(r)} = r_X \left(\frac{1}{T_s}\int_{t-T_s}^{t} (\Delta i_X)^2 d\tau \right) = r_X \langle \Delta i_X \rangle_{T_s,rms}^2. \tag{8}$$

where $\langle \Delta i_X \rangle_{T_s,rms}$ is the element current ripple rms value over a switching period.

Finnaly, after determining the losses expressions over the switching period, it is possible to determine the conductions losses over a line period T_e, which is the effective losses to design and to evaluate the converter components. This can be computed with

$$P_X = \frac{1}{T_e}\int_{t-T_e}^{T_e} \langle p_X \rangle_{T_s} d\tau. \tag{9}$$

The main difference with the simplified losses is the resistive term due to the current ripple rms value, which is defined over a line period by

$$\Delta I_{X,rms} = \sqrt{\frac{1}{T_e}\int_{t-T_e}^{T_e} \langle \Delta i_X \rangle_{T_s,rms}^2 d\tau}. \tag{10}$$

In the following, the current ripple will be evaluated for different circuit components, i.e., line inductor, MOSFET based VSC and IBGT/diode based VSC, of the VSC and how it changes regarding the employed modulation strategy. In this version of the paper it is only presented for the modulations, namely, SVM and DPWM 1 [9], whereas other modulation strategies will be considered in the final version of this work.

III. Current Ripple Analysis for Different PWM Strategies

A. Current Ripple in the Phase Current

Let, exemplarily, the circuit for voltage vector $\vec{V}_1$ as decipted in Fig. 3(a). In order to analyze the current ripple of phase current i_a, the equivalent Thevenin circuit for phase a has been determined as shown in Fig. 3(b). The differential equation of this circuit is given by

$$\frac{3}{2}Ri_a + \frac{3}{2}L\frac{di_a}{dt} = e_a - \frac{(e_b + e_c)}{2} - V_{dc}. \tag{11}$$

In order to evaluate the current ripple, it is supposed that $di_a/dt \approx \Delta i_a/\Delta t$ and $i_a = \langle i_a \rangle_{T_s} + \Delta i_a$. Thus, (11) can be rewritten as

$$\Delta i_a = \frac{1}{3(R\Delta t + L)}\left[2e_a - e_b - e_c - 2V_{dc} - 3R\langle i_a \rangle_{T_s}\right]\Delta t, \tag{12}$$

where Δt is the duration time which vector $\vec{V}_1$ has been applied, i.e., $\Delta t = \Delta t_1 = d_1 T_s$. Considering this methodology,

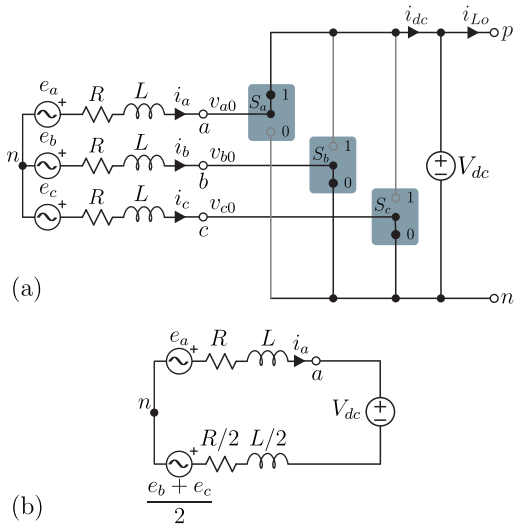

Fig. 3. (a) Equivalent circuit for voltage vector $\vec{V}_1$; and, (b) Equivalent Thevenin circuit for voltage vector $\vec{V}_1$.

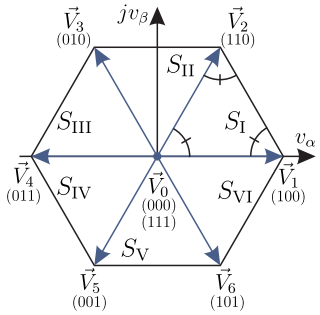

Fig. 4. Switched current i_X waveform in a switching period and its definitions

TABLE I
VOLTAGE VECTORS AND THEIR CORRESPONDANTS CURRENT RIPPLES OF i_a

Voltage Vector	$\Delta i_a[3(R\Delta t_j + L)]$
$\vec{V}_0$	$\left(2e_a - e_b - e_c - 3R\langle i_a\rangle_{T_s}\right)\Delta t_0$
$\vec{V}_1$	$\left(2e_a - e_b - e_c - 2V_{dc} - 3R\langle i_a\rangle_{T_s}\right)\Delta t_1$
$\vec{V}_2$	$\left(2e_a - e_b - e_c - V_{dc} - 3R\langle i_a\rangle_{T_s}\right)\Delta t_2$
$\vec{V}_3$	$\left(2e_a - e_b - e_c + V_{dc} - 3R\langle i_a\rangle_{T_s}\right)\Delta t_3$
$\vec{V}_4$	$\left(2e_a - e_b - e_c + 2V_{dc} - 3R\langle i_a\rangle_{T_s}\right)\Delta t_4$
$\vec{V}_5$	$\left(2e_a - e_b - e_c + V_{dc} - 3R\langle i_a\rangle_{T_s}\right)\Delta t_5$
$\vec{V}_6$	$\left(2e_a - e_b - e_c - V_{dc} - 3R\langle i_a\rangle_{T_s}\right)\Delta t_6$

Table I is presented with the current ripple for all voltage vectors, which vectors are shown in the voltage space vector of Fig. 4. In Table I Δt_j is the correspondent duration time of the voltage vector $\vec{V}_j$.

For a given modulation strategy, the current ripple rms value over a switching period is a composition of the applied voltage vectors. This is formulated as

$$\langle \Delta i\rangle_{T_s,rms} = \sqrt{\frac{1}{T_s}\left\{\int_{\Delta t_1}[\Delta i_1(\tau)]^2 d\tau + \int_{\Delta t_2}[\Delta i_2(\tau)]^2 d\tau + \cdots + \int_{\Delta t_n}[\tag{13}$$

where $\Delta i_n(t)$ is the current ripple function for a given voltage vector applied during the time interval between Δt_n and $\Sigma_n \Delta t_n = T_s$. The current ripple rms value over a switching period of the exemplary current in Fig. 2(a) is given by Fig. 2(b), where the expressions of the current ripple for each part are shown in Fig. 2(c).

Based on the presented procedure and considering the pulse patterns of the PWM strategies SVM and DPWM1 [9], the current ripple rms values over a switching period have been determined. The local expressions for SVM are

$$\begin{aligned}
\langle \Delta i_a\rangle^2_{T_s,rms} &= i_m^2 d_0'/3 + (i_m^2 + i_n^2 + i_m i_n) d_1'/3 + (i_m^2 + i_n^2 - i_m i_n) \\
\langle \Delta i_a\rangle^2_{T_s,rms} &= i_m^2 d_0'/3 + (i_m^2 + i_n^2 - i_m i_n) d_1'/3 + (i_m^2 + i_n^2 + i_m i_n) \\
i_m &= (\Delta i_a|_{\vec{V}_0'})/4, \\
i_n &= i_m + (\Delta i_a|_{\vec{V}_1'})/2,
\end{aligned} \tag{14}$$

and for DPWM1 are

$$\begin{aligned}
\langle \Delta i_a\rangle^2_{T_s,rms} &= i_m^2 d_0'/3 + i_n^2 d_1'/3 + (i_m^2 + i_n^2 + i_m i_n) d_2'/3, \text{for the fi} \\
i_m &= (\Delta i_a|_{\vec{V}_0'})/2, \\
i_n &= -(\Delta i_a|_{\vec{V}_1'})/2, \\
\langle \Delta i_a\rangle^2_{T_s,rms} &= i_m^2 d_0'/3 + (i_m^2 + i_n^2 + i_m i_n) d_1'/3 + i_n^2 d_2'/3, \text{for the se} \\
i_m &= (\Delta i_a|_{\vec{V}_0'})/2, \\
i_n &= -(\Delta i_a|_{\vec{V}_2'})/2,
\end{aligned} \tag{15}$$

where the sextants are defined as in Fig. 1(c), the duty-cycle functions d_1' and d_2' are given in Tab. II, and the value of the zero sequence signal is $d_0' = 1 - d_1' - d_2'$. In Tab. II the $\alpha\beta$ duty-cycle functions are given by an ac current control system or, if a linear load is considered, by an open-loop modulator. Considering the steady state single-phase equivalent circuit of the converter referred to the ac-side shown in Fig. 5(a), where all variables are sinusoidal and defined by

$$\vec{e}_{abc} = E_{pk}[\ \cos(\omega_e t) \quad \cos(\omega_e t - 2\pi/3) \quad \cos(\omega_e t + 2\pi/3)\ ]^T, \tag{16}$$

$$\vec{v}_{abc} = V_{pk}[\ \cos(\omega_e t - \phi_v) \quad \cos(\omega_e t - \phi_v - 2\pi/3) \quad \cos(\omega_e t - \phi_v + 2\pi/3) \tag{17}$$

and

$$\langle \vec{i}_{abc}\rangle_{T_s} = I_{pk}[\ \cos(\omega_e t - \phi_i) \quad \cos(\omega_e t - \phi_i - 2\pi/3) \quad \cos(\omega_e t - \phi_i + 2\pi/3 \tag{18}$$

where E_{pk}, V_{pk} and I_{pk} are the peak values of the input phase voltage, converter phase voltage and phase current, respectively; $\omega_e = 2\pi f_e$ and $f_e = 1/T_e$ are the electrical frequencies; the abc vectors contains information regarding all phases, as given by $\vec{x}_{abc} = [x_a\ x_b\ x_c]^T$; and, ϕ_v and ϕ_i are the displacement angles between the input voltage and the converter voltage and phase current, respectively. These relations are illustrated by the phasor diagram in Fig. 5(b). Thus, the modulation functions can be determined with $\vec{m}_{abc} = \vec{v}_{abc}/V_{dc}$. Employing the Clarke Transformation shown in

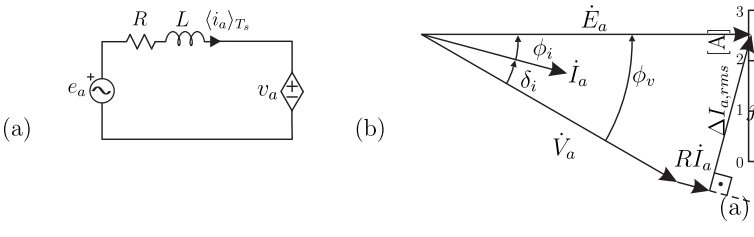

Fig. 5. (a) Steady state single-phase equivalent circuit of the converter referred to the ac-side; (b) Phasor diagram for steady state operation of (a); and, (c) Clarke Transformation matrix used in this work.

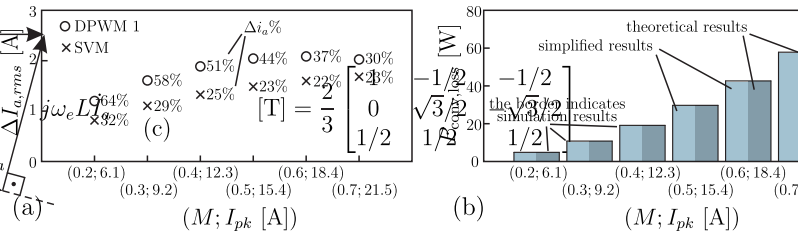

Fig. 6. (a) Phase current ripple rms value for the simulated conditions with SVM and DPWM 1. The percentual ondulation is determined with $\Delta i_a\% = (\max(\Delta i_a)/I_{pk})100\%$; Converter losses for (b) SVM; and, (c) DPWM 1. The converter has been simulated considering the following parameters: $f_e = 60$ Hz; $R = 1\ \mu\Omega$; $L = 460\ \mu$H; $V_{dc} = 760$ V; $f_s = 19.96$ kHz (f_s for SVM and $(3/2)f_s$ for DPWM 1); $E_{pk} = MV_{dc}/\sqrt{3}$; and, the rated condition of 10 kW is determined at $M = 0.7$ and $I_{pk} = 21.5$ A.

TABLE II
RELATIONSHIP BETWEEN THE DUTY-CYCLE FUNCTIONS OF THE VECTORS AND THE $\alpha\beta$ DUTY-CYCLE FUNCTIONS

Sextants	Vector's Duty-cycle Functions	
	d'_1	d'_2
S_{I}	$d_1 = (3/2)(d_\alpha - 1/\sqrt{3}d_\beta)$	$d_2 = \sqrt{3}d_\beta$
S_{II}	$d_2 = (3/2)(d_\alpha + 1/\sqrt{3}d_\beta)$	$d_3 = -(3/2)(d_\alpha - 1/\sqrt{3}d_\beta)$
S_{III}	$d_3 = \sqrt{3}d_\beta$	$d_4 = -(3/2)(d_\alpha + 1/\sqrt{3}d_\beta)$
S_{IV}	$d_4 = -(3/2)(d_\alpha - 1/\sqrt{3}d_\beta)$	$d_5 = -\sqrt{3}d_\beta$
S_{V}	$d_5 = -(3/2)(d_\alpha + 1/\sqrt{3}d_\beta)$	$d_6 = (3/2)(d_\alpha - 1/\sqrt{3}d_\beta)$
S_{VI}	$d_6 = -\sqrt{3}d_\beta$	$d_1 = (3/2)(d_\alpha + 1/\sqrt{3}d_\beta)$

Fig. 5(c) and considering $V_{pk} = (M/\sqrt{3})V_{dc}$, where M is the modulation index, whose range is between 0 and 1, the modulation functions in the $\alpha\beta$ plane are given by

$$\vec{m}_{\alpha\beta} = (M/\sqrt{3})[\ \cos(\omega_e t - \phi_v) \quad \sin(\omega_e t - \phi_v)\ ]^T, \quad (19)$$

which the duty-cycle functions are related with $\vec{d}_{\alpha\beta} = \vec{m}_{\alpha\beta}$. In Fig. 4 the main signals of each modulation strategy are illustrated for a line period, where $d_a = m_a + d_0$ is the duty-cycle function of S_{ap} (and, for the equivalent switch S_a as shown in Fig. 3(a)).

An analytical approximation of the phase current ripple rms value can be determined considering that $R \approx 0$, $\vec{v}_{abc} = \vec{e}_{abc}$ and $\phi_i = 0$, thus for SVM

$$\Delta I_{a,rms} = \frac{MV_{dc}}{48Lf_s}\sqrt{\frac{24\pi - 128M + 9M^2(4\pi - 3\sqrt{3})}{3\pi}} \quad (20)$$

and for DPWM 1

$$\Delta I_{a,rms} = \frac{MV_{dc}}{24Lf_s}\sqrt{\frac{48\pi - 8M(8 + 15\sqrt{3}) + 9M^2(4\pi + \sqrt{3})}{6\pi}}. \quad (21)$$

These theoretical results are in agreement with the results presented in [4], [5], where experimental results [5] are also shown. A more detailed analysis is not the objective of this work, whereas it might be necessary to employ numerical methods in order to determine the current ripple rms values for a given generic application.

B. Current Ripple in the Power Semicondutors

Considering the implementation of the switches in the VSC is SiC MOSFET based, where synchronous rectification is considered as the gate-drive pulse signal strategy, i.e., the current flows through the MOSFET channel. The switch model is reduced as a resistor $R_{S,on}$ for state 1 and as an open-circuit for state 0. Thus, the current that flows throught the switch S_{ap} is given by $i_S = i_a.s_{ap}$, where s_{ap} is the switching function of S_{ap} (cf. Fig. 1(a)) given by the comparison of the modulation function d_a and the carrier. Formulating the integral version of i_S, it can be shown, for all considered pwm strategies, that

$$I_{S,rms} = \sqrt{\frac{I_{pk}^2}{4} + \frac{\Delta I_{a,rms}^2}{2}}, \quad (22)$$

i.e., it is the total rms value of the phase current divided by $\sqrt{2}$.

In the final version of this work the implementation of the switches with IBGTs and anti-parallel diodes will be considered.

IV. ANALYSIS OF THE RESULTS

A comparison of the proposed method with the simplified method, which does not take into account the current ripple, and simulations results on switched models is performed in order to evaluate the accuracy of the presented methodology. The system parameters are given in the caption of Fig. 6, where SiC MOSFETs have been considered to implement the switches (CREE CMF20120D) with $R_{S,on} = 0.11\ \Omega$. The simulated values and the theoretical results of the phase current ripple rms value are very close in all operation conditions (the error is less than 0.1% for SVM and 0.4% for DPWM 1). Thus, only the simulation results are given as shown in Fig. 6(a) for both considered PWM strategies. The converter losses are the most important results obtained from the current rms values. A comparison between the methodologies are presentend in Fig. 6(b)and Fig. 6(c) for SVM and DPWM 1, respectively. It can be seen that the simplified results provides close results, but the differences with the simulation results are bettween 1.1% and 3.6% for SVM; and, 2.6% and 11.5% for DPWM 1. The results are significantly improved considering the proposed methodology, where all results present an error less than 0.6%.

V. Conclusions

This works presented a methodology to improve the calculation of the current ripple rms value in the VSC with different PWM strategies. It has been shown that the semiconductor losses estimations can also be improved considering simpler results in the analysis of the current ripple. The final version of ths work will be enriched with further information.

References

[1] U. Drofenik and J. W. Kolar, "A general scheme for calculating switching and conduction losses of power semiconductors in numerical circuit simulations of power electronic systems," Niigata, Japan, 2005, pp. 4–8.

[2] M. Schweizer, I. Lizama, T. Friedli, and J. W. Kolar, "Comparison of the chip area usage of 2-level and 3-level voltage source converter topologies," in *IEEE 36th Ann. Conf. Ind. Electron., Control and Instrumentation (IECON)*, Glendale, AZ, 2010, pp. 391–396.

[3] J. Liu, W. Chen, J. Zhang, D. Xu, and F. C. Lee, "Evaluation of power losses in different ccm mode single-phase boost pfc converters via a simulation tool," in *IEEE 36th Conf. Rec. of the Ind. Applicat. Soc. Ann. Meeting*, vol. 4, Chicago, IL, 2001, pp. 2455–2459.

[4] J. W. Kolar, H. Ertl, and F. C. Zach, "Influence of the modulation method on the conduction and switching losses of a pwm converter system," *IEEE Trans. Ind. Appl.*, vol. 27, no. 6, pp. 1063–1075, 1991.

[5] A. M. Hava, R. J. Kerkman, and T. A. Lipo, "A high-performance generalized discontinuous pwm algorithm," *IEEE Trans. Ind. Appl.*, vol. 34, no. 5, pp. 1059–1071, 1998.

[6] D. Jiang and F. Wang, "Variable switching frequency pwm for three-phase converters based on current ripple prediction," *IEEE Trans. Power Electron.*, vol. 28, no. 11, pp. 4951–4961, 2013.

[7] ——, "Current-ripple prediction for three-phase pwm converters," *IEEE Trans. Ind. Appl.*, vol. 50, no. 1, pp. 531–538, 2014.

[8] R. W. Erickson and D. Maksimovic, *Fundamentals of Power Electronics*. New York, NY: Kluwer Academic/Plenum Publishers, 2001, vol. 2nd Ed.

[9] D. G. Holmes and T. A. Lipo, *Pulse Width Modulation for Power Converters (Principles and Practice)*. Piscataway, NJ: John Wiley & Sons, Inc., 2003.